Građevinski materijali i konstrukcije
Building Materials and Structures

journal homepage: www.dimk.rs

doi: 10.5937/GRMK2301055T UDK: 699.841
Technical paper

Evaluation of models of the flexural response of rectangular reinforced concrete columns in the post-capping region

Milena Tomić[*1)], Anže Babič[1)], Tatjana Isaković[1)]

[1)] *University of Ljubljana, Faculty of Civil and Geodetic Engineering, Ljubljana, Slovenia*

Article history

Received: 05 December 2022
Received in revised form: 30 January 2023
Accepted: 06 February 2023
Available online: 30 March 2023

Keywords

lumped plasticity model;
near-collapse rotation;
trilinear moment–rotation backbone;
quadrilinear moment–rotation backbone;
post-capping stiffness

ABSTRACT

Simulating the seismic behaviour of a structure up to the point of collapse is an established approach to assessing structural safety during strong earthquakes. In the case of reinforced concrete columns with a predominantly flexural response, a lumped plasticity model with a predefined backbone and Takeda hysteresis rules is often used for this purpose. The present study investigates different moment–rotation backbone models to identify procedures that adequately predict the post-capping part of the backbone. In the first part of the paper, Eurocode 8 procedures for estimating the rotation in the near collapse limit state are reviewed and used to calculate the near collapse rotation of two experimentally tested columns with different levels of confinement. The procedure that agrees best with the experiments is used in the second part of the study, where several options for modelling the post-capping part of the moment–rotation backbone are studied. The results suggest that a quadrilinear moment–rotation backbone with a bilinear post-capping region combined with anearcollapse rotation determined according to the empirical procedure from the current version of Eurocode 8/3 can predict the cyclic response of both poorly and well-confined columns.

1 Introduction

The lumped plasticity modelling approach is commonly used to study the seismic performance of reinforced concrete structures. The Giberson lumped plasticity model is often used forreinforced concrete columns with a predominantly flexural response. In this model, the plastic hinge is defined as a rotational spring having an approximate moment–rotation relationship, defined by the backbone and hysteresis rules, such as the Takeda hysteresis rules [1]. This well-established approach has been used for decades to assess the nonlinear response of reinforced concrete structures (e.g. [2, 3, 4, 5]) and is still relevant today, as researchers are looking for simple and effective models to be used in seismic risk assessment studies (e.g. [6, 7, 8]).

Different models for estimating the moment–rotation backbone have been used previously. The parameters defining the response up to the capping point have been successfully estimated, as this part of the backbone has been well studied (e.g. [9, 10]). However, the response after the capping point, characterised by stiffness and strength degradation, is less well studied. This part of the backbone is important in risk assessment studies, where the seismic behaviour of the structure is simulated up to the point of collapse (e.g. [11, 12, 13]). In the recent literature, researchers have suggested modifications to existing backbone models to better describe the post-capping region (e.g. [6, 14, 15]). These models are often consistent with the backbone as defined in the ASCE/SEI 41 standard [16]. However, the number of studies developing a backbone model consistent with the requirements of the Eurocode standards is more limited.

In the Eurocode 8 standard, the post-capping region is defined by the near collapse (NC) limit state, which is when the flexural strength drops by 20%. Consistent with the code, some studies have defined the moment–rotation backbone in the post-capping region as the NC moment and rotation combined with the assumed post-capping stiffness [17, 18]. The ability to predict the nonlinear response of reinforced concrete elements up to the NC limit state has also been confirmed by the results of pseudodynamic tests (e.g. [19]). However, such a modelling approach is not straightforward, as several different procedures for calculating the NC limit state rotation are included in Eurocode 8. In addition, there are no guidelines for defining the post-capping part of the backbone based on the NC rotation. Several modelling strategies have been proposed. Although most studies predict constant post-capping stiffness [17, 20, 21, 22], some recommend that this part of the backbone should be modelled as bilinear (e.g. [14, 23, 24]).

The present study addresses the lack of guidelines for defining the post-capping part of the moment–rotation backbone consistently with the Eurocode standards. In particular, the aim of the study is to identify a reliable

* Corresponding author:
E-mail address: Milena.Tomic@fgg.uni-lj.si

Eurocode-conforming backbone model that could be used to simulate the post-capping response of rectangular reinforced concrete columns with a predominantly flexural response up to the point of collapse, regardless of the column design level. In the first part of the paper, Eurocode 8 procedures for assessing the NC limit state rotation are reviewed (Section 2) and evaluated against the results of experiments on two rectangular reinforced concrete columns with different levels of confinement (Section 3). The procedure that agreed best with the experiments on both columns is used in the second part of the study (Section 4), where several different models of the moment–rotation backbone are studied and compared to the experimentally obtained cyclic response.

2 Estimation of the NC limit state according to Eurocode 8

Eurocode 8 defines the onset of limit states of reinforced concrete columns by their chord rotations. The chord rotation corresponding to the NC limit state is referred to as the "ultimate chord rotation" in Eurocode 8 (in this paper, the "NC rotation") and can be determined using different procedures. These procedures are first briefly summarised in Subsection 2.1 and then presented in more detail in Subsections 2.2, 2.3 and 2.4. In Subsection 2.2, the material parameters for section analysis are summarised, Subsection 2.3 covers the estimation of the plastic hinge length, and Subsection 2.4 covers the NC rotation calculation.

2.1 Summary of Eurocode 8 procedures

This study considered five Eurocode 8 procedures for assessing the NC rotation of reinforced concrete columns (Table 1). The procedures included in Eurocode 8/3 [25], Eurocode 8/2 [26], and Eurocode 8/1 [27] were considered.

Two procedures in the current Eurocode 8/3 (denoted as EC8/3a&EC2 and EC8/3a) are categorised as analytical, requiring the assessment of the ultimate curvature using section analysis, while the third procedure (denoted as EC8/3b) is semi-empirical; section analysis is not needed. The EC8/3a&EC2 procedures follow the requirements of Eurocode 2 [28] when performing section analysis,while EC8/3a follows the rules included in Eurocode 8/3. The analytical and empirical procedures differ regarding the required data. The analytical procedures require an advanced definition of the materials and an estimate of the plastic hinge length. These data are not needed in the empirical approach.

The procedure included in Eurocode 8/2 (denoted as EC8/2) is also analytical. It is similar to the analytical procedures from Eurocode 8/3 but uses different assumptions for section analysis and plastic hinge length.

The procedure from the draft of the new Eurocode 8/1 (denoted as prEC8/1) combines the analytical and empirical approaches. The yield rotation is estimated by performing section analysis, while the ultimate (NC) rotation is estimated using a semi-empirical approach. This procedure is specified only for rectangular cross-sections. For other types of cross-sections not investigated in this study, the new Eurocode 8/1 prescribes an analytical approach.

2.2 Material parameters and section analysis

The analytical approaches require the estimation of yield and ultimate curvatures as input data for calculating the NC rotation (Table 1). They are defined by section analysis. Section analysis is typically performed by discretizing the cross-section into fibres associated with the corresponding materials: unconfined concrete cover, confined concrete core, and longitudinal reinforcement steel. While the constitutive law of unconfined concrete is the same for all procedures considered in this study, the constitutive law of confined concrete varies from procedure to procedure (Table 2). The constitutive laws for longitudinal reinforcement steel (Table 3) also differ, mainly regarding the value of the ultimate strain considered.

In general, procedure prEC8/1 requires section analysis only to determine the yield curvature (for yield rotation calculation), because the post-yield response is determined empirically. Moreover, the new Eurocode 8/1 distinguishes between two cases: failure of the section before and after the concrete cover spalling.

In order to determine which case governs the response, the section analysis should be initially performed assuming that the section failure occurs after the spalling of the concrete cover. The flexural resistance of the concrete core, defined as the moment corresponding to the ultimate strain in the confined core or longitudinal reinforcement, should then be compared to the total flexural resistance. The latter is determined as the maximum moment that developed before the spalling of the concrete cover. If the flexural resistance of the concrete core is higher than 80 % of the total flexural resistance, the assumption that the section fails after the spalling is confirmed. Otherwise, the section analysis should be repeated with different ultimate strains, as defined by Eqs. (15) and (20).

Table 1. Requirements of the Eurocode 8 procedures for NC rotation calculation

Procedure	Approach	Section analysis	Advanced material definition ($f_{cc}, \varepsilon_{cc}, \varepsilon_{uc}, \varepsilon_{su}, \ldots$)	Plastic hinge length estimation
EC8/3a&EC2	Analytical	Yes	Yes	Yes
EC8/3a	Analytical	Yes	Yes	Yes
EC8/3b	Empirical	No	No	No
EC8/2	Analytical	Yes	Yes	Yes
prEC8/1	Combined	Yes	Yes	No

Table 2. Summarised Eurocode procedures for the definition of the confined concrete constitutive laws

Procedure	Equations	
EC8/3a&EC2	$f_{cm,c} = \begin{cases} f_{cm} \cdot \left(1 + 5\frac{\sigma_2}{f_{cm}}\right), if\ \sigma_2 \le 0.05 f_{cm} \\ f_{cm} \cdot \left(1.125 + 2.5\frac{\sigma_2}{f_{cm}}\right), if\ \sigma_2 > 0.05 f_{cm} \end{cases}$	(1)
	$\varepsilon_{c2,c} = \varepsilon_{c2}\left(\frac{f_{cm,c}}{f_{cm}}\right)^2$	(2)
	$\varepsilon_{cu2,c} = \varepsilon_{cu2} + 0.2\frac{\sigma_2}{f_{cm}}$	(3)
	$\sigma_2 = \alpha \cdot \rho_{sx} \cdot f_{yw}$	(4)
EC8/3a	$f_{cm,c} = f_{cm} \cdot \left(1 + 0.37\left(\frac{\sigma_2}{f_{cm}}\right)^{0.86}\right)$	(5)
	$\varepsilon_{c2,c} = \varepsilon_{c2}\left(1 + 5\left(\frac{f_{cm,c}}{f_{cm}} - 1\right)\right)$	(6)
	$\varepsilon_{cu2,c} = 0.004 + 0.5\frac{\sigma_2}{f_{cm,c}}$	(7)
	$\sigma_2 = \alpha \cdot \left(min\ (\rho_{wy}; \rho_{wz})\right) \cdot f_{yw}$	(8)
EC8/2	$f_{cm,c} = f_{cm} \cdot \left(2.254\sqrt{1 + 7.94\frac{\sigma_2}{f_{cm}}} - 2\frac{\sigma_c}{f_{cm}} - 1.254\right)$	(9)
	$\varepsilon_{c2,c} = 0.002\left(1 + 5\left(\frac{f_{cm,c}}{f_{cm}} - 1\right)\right)$	(10)
	$\varepsilon_{cu2,c} = 0.004 + 2.8\frac{\sqrt{\rho_{wy} \cdot \rho_{wz}} f_{ym} \varepsilon_{su}}{f_{cm,c}}$	(11)
	$\sigma_2 = \alpha \cdot \sqrt{\rho_{wy} \cdot \rho_{wz}} \cdot f_{yw}$	(12)
prEC8/1	$f_{cm,c} = \begin{cases} f_{cm} + \alpha \cdot 4\sigma_2, if\ \sigma_2 \le 0.6 f_{cm} \\ f_{cm} + \alpha \cdot 3.5\sigma_2^{\frac{3}{4}} f_{cm}^{\frac{1}{4}}, if\ \sigma_2 > 0.6 f_{cm} \end{cases}$	(13)
	$\varepsilon_{c2,c} = 0.002\left(1 + 5\frac{f_{cm,c}}{f_{cm}}\right)$	(14)
	$\varepsilon_{cu2,c} = \begin{cases} \left(\frac{18.5}{h_0(mm)}\right)^2 + 0.04\sqrt{\frac{\alpha \cdot (\rho_{wy} + \rho_{wz}) \cdot f_{yw}}{f_{cm}}}, if\ M_{Rd,0} > 0.8 M_{Rd} \\ \min\left(0.01; \max\left(0.0035; \left(\frac{18.5}{h(mm)}\right)^2\right)\right), if\ M_{Rd,0} \le 0.8 M_{Rd} \end{cases}$	(15)
	$\sigma_2 = \min\left(\rho_{wy} \cdot f_{yw};\ \rho_{wz} \cdot f_{yw}\right)$	(16)

f_{cm},$f_{cm,c}$ – Compressive strength of unconfined and confined concrete
σ_2 – Confining stress
α – Confinement effectiveness factor
$\varepsilon_{c2}, \varepsilon_{c2,c}$– Strain at maximum stress for unconfined and confined concrete
$\varepsilon_{cu2}, \varepsilon_{cu2,c}$ – Ultimate strain of unconfined and confined concrete
$\rho_{wz}, \rho_{wy}, \rho_{sx}$ – Ratio of lateral reinforcement in z- and y-directions and the direction of loading
f_{yw} – Transverse reinforcement strength
$M_{Rd}, M_{Rd,0}$ – Flexural resistance of the entire cross-section and flexural resistance of concrete core

Table 3. Eurocode limits of the ultimate strain in the longitudinal reinforcement

Procedure	Longitudinal reinforcement ultimate strain limitation	
EC8/3a&EC2	$\varepsilon_{su} = \begin{cases} min\left(\varepsilon_{su,exp}, 2.5\ \%\right), for\ ductility\ class\ A \\ min\left(\varepsilon_{su,exp}, 5.0\ \%\right), for\ ductility\ class\ B \\ min\ (\varepsilon_{su,exp}, 6.0\ \%), for\ ductility\ class\ C \end{cases}$	(17)
EC8/3a	$\varepsilon_{su} = \begin{cases} min\ (\varepsilon_{su,exp}, 2.5\ \%), for\ ductility\ class\ A \\ min\ (\varepsilon_{su,exp}, 5.0\ \%), for\ ductility\ class\ B \\ min\ (\varepsilon_{su,exp}, 6.0\ \%), for\ ductility\ class\ C \end{cases}$	(18)
EC8/2	$\varepsilon_{su} = \begin{cases} min\ (\varepsilon_{su,exp}, 2.5\ \%), for\ ductility\ class\ A \\ min\ (\varepsilon_{su,exp}, 5.0\ \%), for\ ductility\ class\ B \\ min\ (\varepsilon_{su,exp}, 7.5\ \%), for\ ductility\ class\ C \end{cases}$	(19)
prEC8/1	$\varepsilon_{su} = \begin{cases} 0.4\varepsilon_{su,exp}, if\ M_{Rd,0} > 0.8M_{Rd} \\ \frac{4}{15}\varepsilon_{su,exp}\left(1 + 3\frac{d_{bl}}{s}\right)(1 - 0.75e^{-0.4N_{b,compr}}), if\ M_{Rd,0} \leq 0.8M_{Rd} \end{cases}$	(20)

$\varepsilon_{su,exp}, \varepsilon_{su}$ – Experimentally obtained and prescribed ultimate strain of longitudinal reinforcement
d_{bl} – Diameter of longitudinal reinforcement bars
s – Distance between stirrups
$N_{b,compr}$ – Number of longitudinal reinforcement bars in compression
$M_{Rd}, M_{Rd,0}$ – Flexural resistance of entire cross-section and flexural resistance of concrete core

2.3 Plastic hinge length

Damage to structural elements is typically limited to the end regions of elements subjected to the largest moments. This region is denoted as the plastic hinge.

The length of the plastic hinge, required in the analytical procedures for estimating the NC rotation, is assessed with the equations given in Table 4. They differ mainly regarding the assumed distribution of plastic deformations along the column.

The selection of a procedure for calculating the plastic hinge length should be consistent with the procedure used for section analysis. Different approaches cannot be combined because they have been calibrated to generate the appropriate ultimate chord rotations.

The equation fromprEC8/1 is presented only for comparison and does not apply to columns with rectangular cross-sections, such as those considered in this study.

Table 4. Plastic hinge length estimation

Procedure	Plastic hinge length	
EC8/3a&EC2	$L_{pl} = 0{,}1L_V + 0{,}17h + 0{,}24\, d_{bl} f_{yl}/\sqrt{f_c}$	(21)
EC8/3a	$L_{pl} = L_V/30 + 0{,}2h + 0{,}11\, d_{bl} f_{yl}/\sqrt{f_c}$	(22)
EC8/2	$L_{pl} = 0{,}1L_V + 0{,}015 d_{bl} f_{yl}$	(23)
prEC8/1	$L_{pl} = \left(1 - 0.45min(0{,}7;\ \nu)\right)\left(1 + 0{,}4min\left(9;\ \frac{L_V}{h}\right)\right) \cdot \left(1 - \frac{1}{3}\sqrt{min\left(2{,}5; max\left(0{,}05; \frac{b}{h}\right)\right)}\right) 0{,}3h$	(24)

L_{pl} – Plastic hinge length
L_V – Shear span
h, b – Cross-section height and width of the compression zone, respectively
d_{bl} – Diameter of the longitudinal reinforcement bars
f_{yl}, f_c – Longitudinal reinforcement and concrete strength, respectively
ν – Axial load level
$*$ not applicable to rectangular cross-sections

2.4 Near collapse rotation

The Eurocode 8 procedures considered in this study use different equations to calculate the NC rotation based on the parameters assessed in previous steps (Table 5). The analytical approaches (EC8/3a & EC2, EC8/3a & EC8/2) estimate the NC chord rotation, θ_{um}, summing the yield rotation, θ_y,and the post-yielding part of the chord rotation corresponding to the yield and ultimate curvatures (see Section 2.2).

The post-yielding part of the NC chord rotation is calculated by assuming a constant post-yield curvature distribution along the entire length of the plastic hinge.

The calculation of the NC chord rotation according to the empirical approach (EC8/3b) is conceptually different. The chord rotation is estimated based on the material, geometrical properties, and axial load ratio of the column.

Last, prEC8/1 combines the analytical and empirical approaches to estimate the yield chord rotation and the post-yielding part of the NC chord rotation, respectively.

Table 5. Summarised Eurocode procedures for calculating the ultimate (NC) rotation

Procedure	Equations	
EC8/3a&EC2	$\theta_y = \varphi_y\,(L_V + \alpha_V z)/3 + 0{,}0014\left(1 + 1{,}5\frac{h}{L_V}\right) + \frac{\varepsilon_y}{d-d'}\frac{d_{bl}f_{yl}}{6\sqrt{f_c}}$	(25)
	$\theta_{um} = \theta_y + (\varphi_u - \varphi_y)L_{pl}\left(1 - \frac{0{,}5L_{pl}}{L_V}\right)$	(26)
EC8/3a	$\theta_y = \varphi_y\,(L_V + \alpha_V z)/3 + 0{,}0014\left(1 + 1{,}5\frac{h}{L_V}\right) + \frac{\varepsilon_y}{d-d'}\frac{d_{bl}f_{yl}}{6\sqrt{f_c}}$	(27)
	$\theta_{um} = \theta_y + (\varphi_u - \varphi_y)L_{pl}\left(1 - \frac{0{,}5L_{pl}}{L_V}\right)$	(28)
EC8/3b	$\theta_{um} = 0{,}016(0{,}3^{\nu})\left[\frac{max\,(0{,}01;\omega')}{max\,(0{,}01;\omega)}f_c\right]^{0{,}225}\left(min\left(9;\frac{L_V}{h}\right)\right)^{0{,}35} 25^{\left(\alpha\rho_{sx}\frac{f_{yw}}{f_c}\right)}1{,}25^{100\rho_d}$	(29)
EC8/2	$\theta_y = \varphi_y L_V/3$	(30)
	$\theta_{um} = \theta_y + (\varphi_u - \varphi_y)L_{pl}\left(1 - \frac{0{,}5L_{pl}}{L_V}\right)$	(31)
prEC8/1	$\theta_y = \varphi_y\,(L_V + (d-d'))/3 + \varphi_\gamma\frac{f_{yl}d_{bl}}{8\sqrt{f_c}} + 0{,}0019\left(1 + \frac{h}{1{,}6L_V}\right)$	(32)
	$\theta_{um} = \theta_y + K\cdot 0{,}016(0{,}2^{\nu})\left[\frac{max\,(0{,}01;\omega')}{max\,(0{,}01;\omega)}\right]^{0{,}25}\left(\min\left(2;\frac{f_c}{25}\right)\right)^{0.1}$ $\left(\frac{1}{25}min\left(9;\frac{L_V}{h}\right)\right)^{0{,}35} 24^{\left(\alpha\rho_{sx}\frac{f_{yw}}{f_c}\right)}0.039$	(33)

θ_y, θ_{um} – Yield and ultimate (NC) rotations
L_{pl} – Plastic hinge length
φ_y, φ_u– Yield and ultimate curvatures
L_V – Shear span
$\alpha_V z = d - d'$ – Tension shift in moment diagram, if the shear cracking happens before the flexural yielding
h – cross-section height
ε_y – Longitudinal reinforcement yield strain
f_{yl}, f_{yw}, f_c – Flexural and transverse reinforcement steel and concrete strength
ν – Axial load level
ω, ω' – Mechanical reinforcement ratio of the tension and compression flexural reinforcements
α – Confinement effectiveness factor
$\rho_{sw}, \rho_{sx}, \rho_d$ – Ratio of lateral reinforcement in the direction of loading, mean in both directions, and diagonal reinforcement
K – Correction factor considering the ductility class (1.0 for DC3, 0.9 for DC2, 0.8 for DC1)

3 Evaluation of Eurocode procedures against experiments

The Eurocode 8 procedures were used to calculate the NC rotations of two experimentally studied cantilever-reinforced concrete columns. The experiments were conducted at the Slovenian National Building and Civil Engineering Institute in cooperation with the University of Ljubljana [23]. By comparing the analysis and experimental data, the best way to estimate how they will respond was found.

The columns considered in this study are described in Subsection 3.1. Analysis and comparison with the experiments are presented in Subsections 3.2, 3.3, and 3.4.

3.1 Description of the columns

Anžlin [23] conducted a series of 1:2 scale cyclic tests on rectangular reinforced concrete columns with varying lateral reinforcement amounts and detailing. The shear span of the columns was 1.8 m, and the axial load level was about 10 % of the designed strength of the concrete section (common for bridge columns). The cross-section height and width were 30 and 40 cm, respectively, while the longitudinal reinforcement ratio was 1%. The concrete grade was C30/37, while the grade of the longitudinal reinforcement steel was S500, and the ductility class was C.

The cyclic horizontal displacement was imposed at the top of the columns in the weaker direction with gradually increasing cycle amplitudes. At each level of amplitude, two cycles were applied in a row while the axial load stayed the same.

One column had standard reinforcement (labeled STD/135) and the other had substandard reinforcement (labeled SUB/90). These two columns were chosen to test the methods described in Section 2. (Fig. 1). Column SUB/90 and STD/135 had a lateral reinforcement ratio of 0.25 % and 0.55 % and stirrups' hook angle of 90° and 135°, respectively.

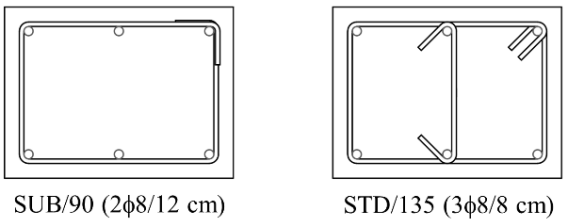

Figure 1. The cross-sections of columns

3.2 Material parameters and section analysis

The section analysis was performed in all cases using OpenSees [29] with a *ZeroLength* fibre section. The section was divided into concrete and steel fibres. Unconfined cover and confined core concrete were considered. They were created with the Concrete04 material. Confined concrete properties were defined according to the procedures presented in Table 2.

The stress–strain relationships for concrete defined according to different procedures are presented in Fig. 2 for columns SUB/90 and SUB/135. All of the procedures result in a similar strength for the confined concrete. However, the ultimate deformations of the confined concrete differ significantly. For both columns, the highest ultimate deformations were obtained using the EC8/2 procedure, while the lowest ultimate deformations resulted from the EC8/3a&EC2 procedure. The ratio between the highest and lowest ultimate deformations is more than 2.

Steel02 was used to model the longitudinal reinforcement. This material does not limit the maximum strain (Table 3). Therefore, it was considered in the post processing stage. Fig 3. shows the longitudinal reinforcement stress–strain relationships for the two columns, together with the limitations of the ultimate strain obtained with different procedures (Table 3). The experimentally obtained ultimate strain is also presented; however, this was obtained under monotonic loading. Thus, it exceeded almost all analytical values.

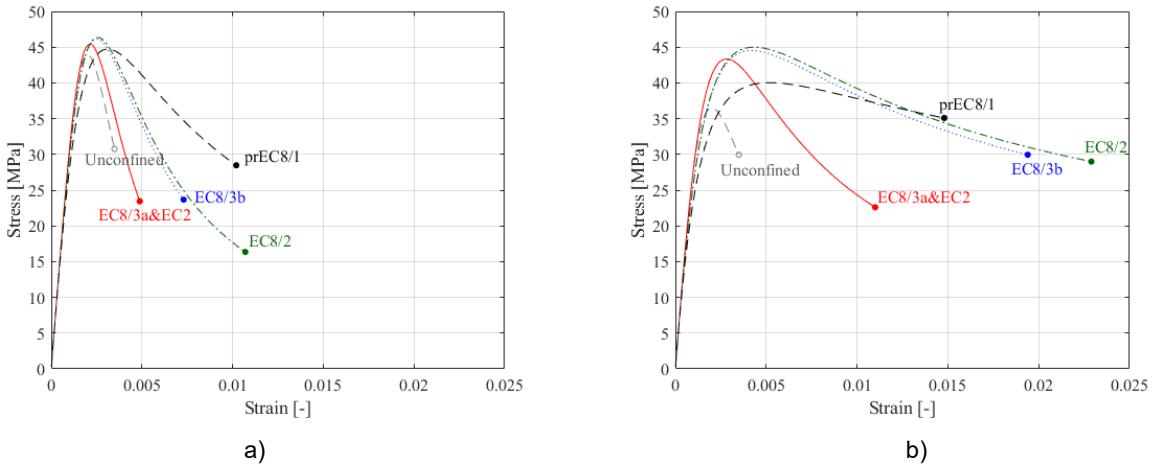

Figure 2. Concrete stress–strain relationships assigned in OpenSees for columns a) SUB/90 and b) STD/135 (compression is positive)

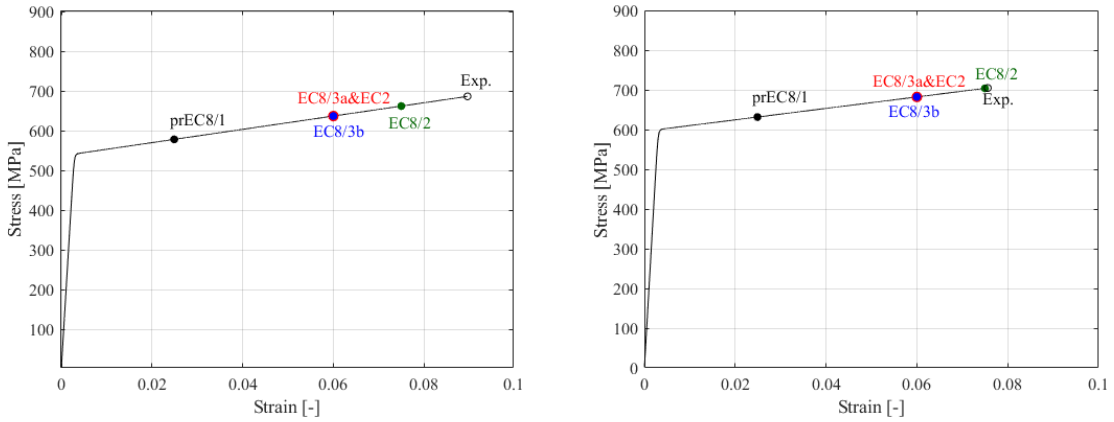

Figure 3. Longitudinal reinforcement stress–strain relationships assigned in OpenSees, Eurocode 8 limitations of the ultimate strain and the experimentally obtained ultimate strain for columns a) SUB/90 and b) STD/135

The moment–curvature relationships were idealised as elastoplastic. Idealisation was performed by assuming the pre-yield stiffness is the secant stiffness at the point where the first yielding of the longitudinal reinforcement occurs, considering the equal surface rule and equalising the areas under the actual and idealised curves.

It was assumed that the ultimate curvature was reached when the ultimate strain was attained either in the confined concrete or in the longitudinal reinforcement. The idealisation of the moment–curvature relationship is illustrated in Fig. 4 for the example of the prEC8/1 procedure for column SUB/90. In this case, the reinforcement failure was identified as critical.

The idealised moment–curvature relationships were determined for both columns and all procedures that use section analysis (Fig. 5). While the strengths were similar in all cases, the maximum curvatures obtained with the considered procedures differed significantly. According to all procedures except for prEC8/1, the ultimate curvature of column SUB/90 was governed by the ultimate strain of the confined concrete. In column STD/135, only the EC8/3a&EC2 procedure predicted that the concrete failure was critical.

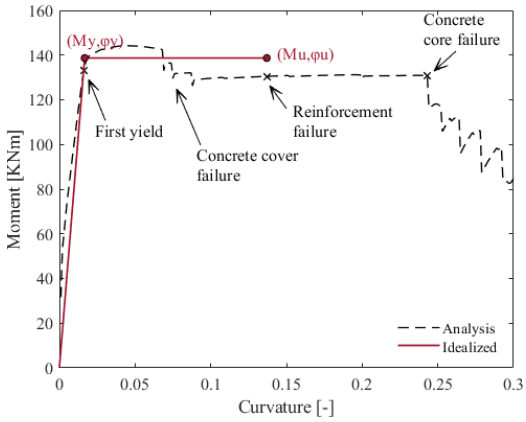

Figure 4:An example of the idealisation of the moment–curvature relationship

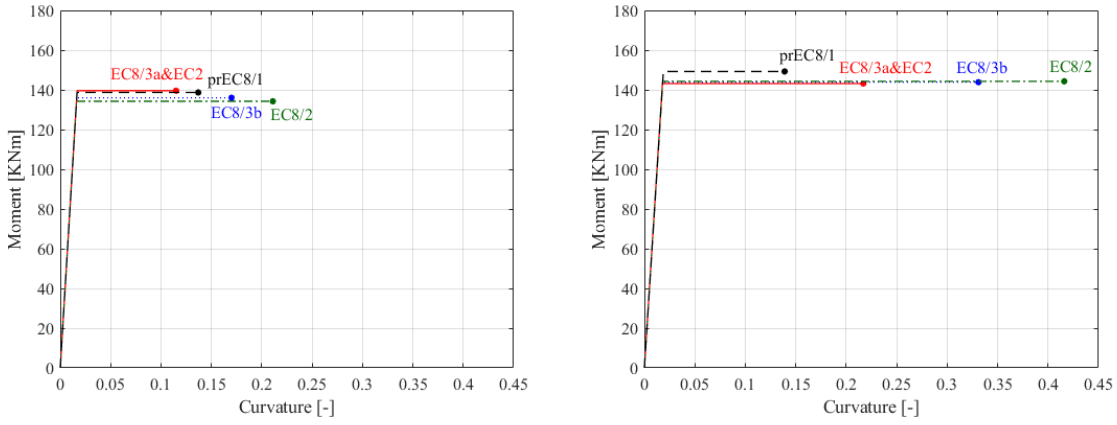

Figure 5. The idealised moment–curvature relationships for columns a) SUB/90 and b) STD/135

3.3 Plastic hinge length

Another parameter that influences the ultimate chord rotation is the plastic hinge length. Plastic hinge lengths of two considered columns obtained with different procedures (see Table 4) are summarised in Fig. 6. The results are presented only for the analytical approaches. The largest values were obtained with procedure EC8/3a&EC2, which amounted to about twice the height of the cross-section. According to the other two theoretical procedures, the plastic hinge length was about two times smaller.

3.4 Near collapse rotation – comparison with experiments

The NC rotations were calculated using the equations in Table 5 and compared to the experimental results. Figs. 7 and 8 compare columns SUB/90 and STD/135, respectively.

In SUB/90, the measured NC collapse rotation (corresponding to a 20 percent loss of flexural strength) was 5.5 percent. All the procedures, except EC8/3&EC2, matched the experimental data very well.

In column STD/135, the measured NC chord rotation was 7.5 %. The analytical procedures (EC8/3a and EC8/2) that predicted the NC rotation of the poorly confined column SUB/90 significantly overestimated the NC rotation. The NC rotation predicted by the empirical procedure EC8/3b was slightly lower than the measured one. The analytical procedure EC8/3a&EC2 and the combined procedure prEC8/1 were the most conservative.

The comparison of NC rotations obtained with Eurocode 8 procedures showed that the empirical procedure in the current version of Eurocode 8/3 could adequately estimate the NC rotation for both poorly and well-confined columns. Therefore, this procedure was considered in the second part of this study (Section 4), where different approaches for modelling the entire post-capping flexural response were analysed.

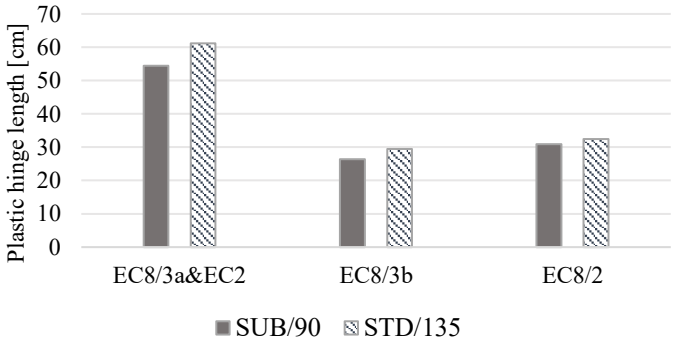

Figure 6. The estimated plastic hinge lengths for the analysed columns

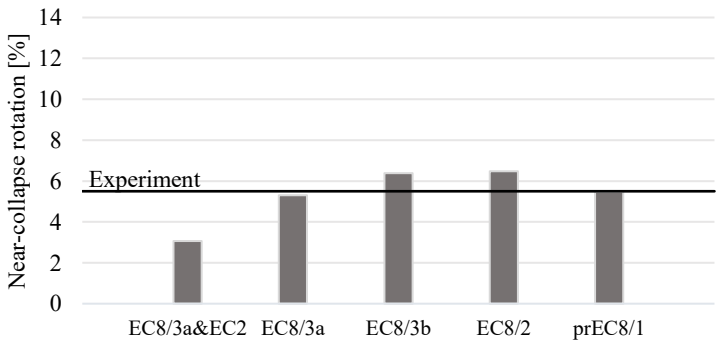

Figure 7. Comparison of predicted NC rotations with experimentally determined value for column SUB/90

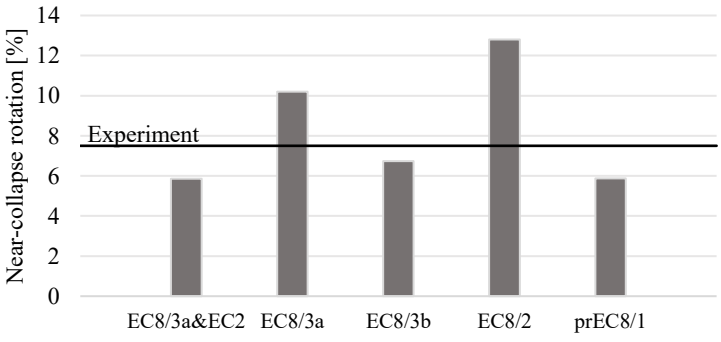

Figure 8. Comparison of the predicted NC rotations with experimentally determined value for column STD/135

4 Moment–rotation relationship for lumped plasticity models

The moment–rotation backbone of plastic hinges is one of the key features of lumped plasticity models. Different procedures to define the backbone are available. The backbone is typically considered trilinear (e.g. [17, 20, 22]), having an initial elastic branch, a plastic branch, and a post-capping branch (Fig. 9a).

The trilinear model can be refined by increasing the number of branches, which may increase the generality of the model but also make it more difficult to calibrate. As this study focused on the post-capping part of the backbone, the impact of increasing the number of branches in that region was explored. An example of such a backbone is the quadrilinear moment–rotation model with a bilinear post-capping response (Fig. 9b) proposed by Anžlin [23]. In the present study, both types of backbone models, trilinear and quadrilinear, were evaluated and compared to the results of the experiments presented in Section 3.1.

4.1 Trilinear moment–rotation backbone

The trilinear moment–rotation backbone (Fig. 9a) can be defined by three characteristic points. In this study, the first two characteristic points corresponded to the yield (Y) and NC limit states.

The rotations at these limit states were defined according to the empirical approach included in the current version of Eurocode 8/3 (see Subsection 2.4). Following the typical procedures reported in the literature, the capping (Cap) point and the total collapse (TC) point were obtained based on the slope of the post-capping branch of the backbone curve. In their evaluation of a code-compliant structure, Žižmond et al. [30] defined the post-capping slope as a ratio of 3.5 between the rotation at the TC point and the rotation at the Cap point (Model T1 in Table 6). This value is consistent with the observations Dolšek [31], which showed that the ratio between the TC and Cap rotations in backbone models is usually between 3 and 4.

In another study, Kreslin and Fajfar [22] have analysed an older structure and defined the post-capping slope based on a ratio between the plastic parts of the TC and NC rotations ($k_{pl,TC/NC}$) equal to 2.0 (Model T2 in Table 6). Comparing these two studies suggests that the post-capping stiffness is affected by the level of design. Consistent with this observation, Anžlin [23] has proposed an equation for determining $k_{pl,TC/NC}$ based on the effective mechanical volumetric confinement ratio in the column, $\omega_\alpha = \alpha\rho_w f_{yw}/f_c$ (Model T3 in Table 6):

$$k_{pl,TC/NC} = min(-0.02\omega_\alpha(\%) + 1.55 \geq 1; 1.34) \qquad (34)$$

In Model T3, $k_{pl,TC/NC}$ was equal to the upper bound (1.34) for both columns.

Three different models of the trilinear moment–rotation backbone were defined by considering these three approaches. The corresponding moments were calculated using the section analysis described in Subsection 2.2 and the following assumptions: moments M_Y and M_{Cap} were assumed to be equal to the maximum moment from the section analysis, moment M_{NC} was assumed to be 80 % of M_{Cap}, and moment M_{TC} was assumed to be 0. Moreover, the rotations at points Y and NC (see Fig. 9) were considered equal to rotations θ_y and θ_{um}, respectively. They were defined according to the Eurocode 8/3 empirical procedure (see Subsection 2.4).

The moment–rotation backbones were calculated for the two tested columns (Subsection 3.1) and compared to the experimentally obtained cyclic responses (Fig. 10). All three backbone models intersect at the NC point, one of the modelling assumptions. At this point, the models matched well with the experimental results, which is a direct consequence of the capability of the Eurocode 8/3 empirical procedure to predict the NC rotation.

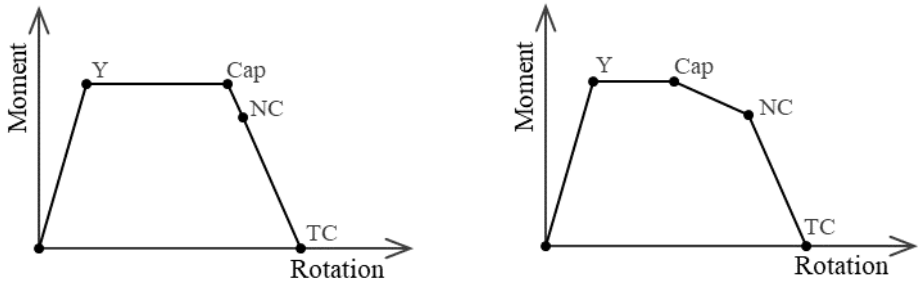

a) **b)**

Figure 9. Moment–rotation backbone models: a) trilinear and b) quadrilinear

Table 6. Characteristic points of trilinear moment–rotation backbone models

Model	Characteristic point	Rotation
Model T1	Cap	$\theta_{Cap} = \theta_{NC}/1.5$
	TC	$\theta_{TC} = 3.5\theta_{Cap}$
Model T2	Cap	$\theta_{Cap} = 1.25\theta_{NC} - 0.25\theta_{TC}$
	TC	$\theta_{TC} = \theta_Y + 2.0(\theta_{NC} - \theta_Y)$
Model T3	Cap	$\theta_{Cap} = 1.25\theta_{NC} - 0.25\theta_{TC}$ $\quad k_{pl,TC/NC} = 1.34$
	TC	$\theta_{TC} = \theta_Y + k_{pl,TC/NC}(\theta_{NC} - \theta_Y)$ (SUB/90 and STD/135)

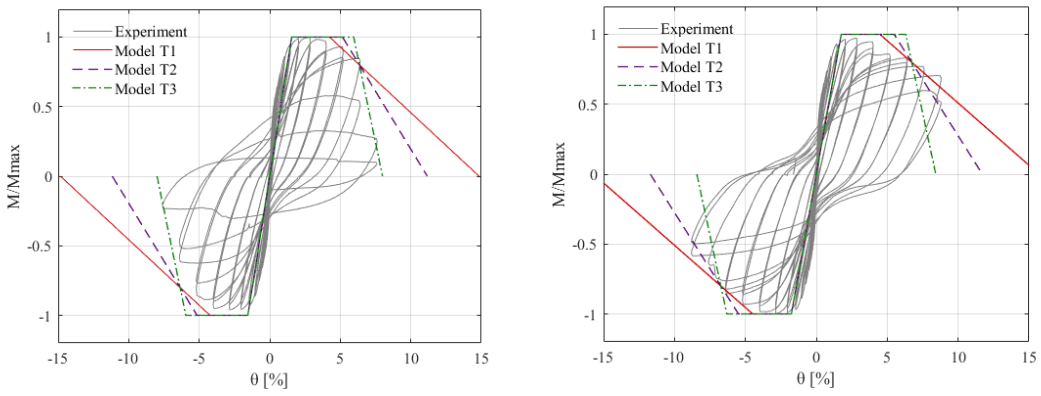

Figure 10. Comparison of trilinear moment–rotation backbones for columns a) SUB/90 and b) STD/135

Model T1 and Model T2 provided a fair prediction of the post-capping region up to the NC point for both columns. This result was expected because these models were originally proposed for such purposes. However, Model T3 gives the best prediction for the poorly confined column from the NC point on. However, none of the trilinear backbone models was suitable for modelling the entire post-capping region of both columns.

4.2 Quadrilinear moment–rotation backbone

In order to better match the post-capping response with the experimental results, four quadrilinear moment–rotation backbone models were also defined (Fig. 9b). The definition of quadrilinear backbone models includes an additional characteristic point as an independent parameter. The Cap point, which has already been addressed, was used as this additional fourth characteristic point. For all quadrilinear backbone models, the capping rotation was calculated according to the empirical procedure proposed by Haselton [10]:

where v is the level of axial load, f_c is the concrete compressive strength, ρ_l is the longitudinal reinforcement ratio, ρ_{sx} is the ratio of lateral reinforcement in the direction of loading, and α_{sl} is an indicator of the possibility of bond–slip. The moment corresponding to the Cap point was considered equal to the maximum moment from the section analysis in the same manner as for the trilinear backbone (Subsection 4.1). Moreover, the same moments and rotations corresponding to the Y and NC points were used as for the trilinear backbone.

Four quadrilateral models with different post-NC branches were considered (see Table 7 and Fig. 11). Models Q1 and Q2 were defined based on the same assumptions as the trilinear backbone models (Subsection 3.1). In Model Q3, the rotation at the TC point was obtained using the ratio between the rotation at the TC point and the Cap point ($k_{TC/Cap}$) proposed by Anžlin [23], specifically for application to quadrilinear backbones:

$$\theta_{Cap} = 0.12(1 + 0.4\alpha_{sl})(0.2)^{v}(0.02 + 40\rho_{sx})^{0.52}(0.56)^{0.01f_c}(2.37)^{10\rho_l} \quad (35)$$

$$k_{TC/Cap} = min(0{,}19\omega_{\alpha}(\%); -0{,}02\omega_{\alpha}(\%) + 6.86; 4) \quad (36)$$

Table 7. Characteristic points of quadrilinear moment–rotation backbone models

Model	Characteristic point	Rotation	
Model Q1	Cap	$\theta_{Cap} - from\ Eq.14$	
	TC	$\theta_{TC} = 3.5\theta_{Cap}$	
Model Q2	Cap	$\theta_{Cap} - from\ Eq.14$	
	TC	$\theta_{TC} = \theta_Y + 2.0(\theta_{NC} - \theta_Y)$	
Model Q3	Cap	$\theta_{Cap} - from\ Eq.14$	$k_{TC/Cap} = 2.1\ (SUB/90)$
	TC	$\theta_{TC} = k_{TC/Cap}\theta_{Cap}$	$k_{TC/Cap} = 3.2\ (STD/135)$
Model Q4	Cap	$\theta_{Cap} - from\ Eq.14$	
	TC	$\theta_{TC} - from\ Eq.16$	

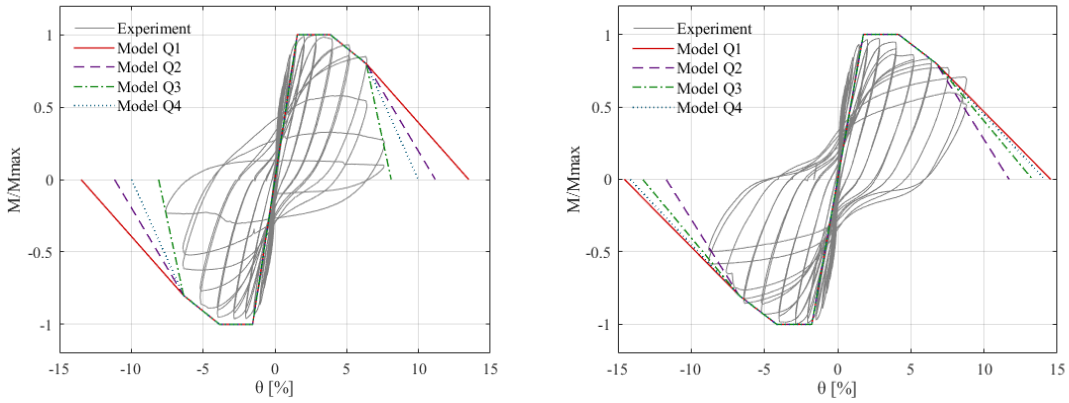

Figure 11. Comparison of quadrilinear moment–rotation backbones for columns a) SUB/90 and b) STD/135

In Model Q4, the rotation at the TC point was obtained using an empirical expression for post-capping rotation capacity developed by Haselton [10]:

$$\theta_{TC} = \theta_{Cap} + 0.76(0.031)^{\nu}(0.02 + 40\rho_{sx})^{1.02} \leq \theta_{Cap} + 0.1 \quad (37)$$

This model was selected by considering the capping rotation model (Eq. (35)) proposed by the same author. Eqs. (35) and (37) were originally proposed for use in combination with the Ibarra hysteresis model [20]. This model accounts for history-dependent strength and stiffness deterioration, which is not the case in the present study.

The quadrilinear moment–rotation backbones are compared with the experimental data in Fig. 11. In the poorly confined column, the post-capping response was very accurately predicted by Model Q3, while the other three models overestimated the TC rotation. The experimental response of the well-confined column was simulated very well by Models Q1, Q3 and Q4. The model Q2 slightly underestimated the moments after the NC point. This outcome was expected because Model Q2 was originally used to predict the post-capping response of columns that did not meet the requirements of Eurocode. Model Q3 was found to be the most general and suitable for predicting the post-capping response of both poorly and well confined columns based on these findings.

4.3 Application of the quadrilinear moment–rotation backbone model

The best match with the experimental results was obtained with the quadrilinear backbone model (see Fig. 11b) defined by: (i) the Cap rotation calculated according to Haselton [10], (ii) the NC rotation determined according to the empirical Eurocode 8/3 procedure [25], and (iii) the TC rotation as proposed by Anžlin [23]. Therefore, this model was chosen for the simulation of the cyclic experiments. The experiments were numerically simulated in the *OpenSees* software [29]. The columns were modelled with the Giberson lumped plasticity model. A nonlinear ZeroLength element was used at the base to model the nonlinear response. The rest of the column was represented by an infinitely stiff and elastic element.

The cyclic behaviour of the nonlinear element was modelled using the *TakedaDAsym* material [32] which follows the Takeda hysteresis rules [1] and considers a quadrilinear moment–rotation backbone. The analytical and experimental cyclic responses are compared in Fig. 12. They had a good match for both the poorly and well confined columns.

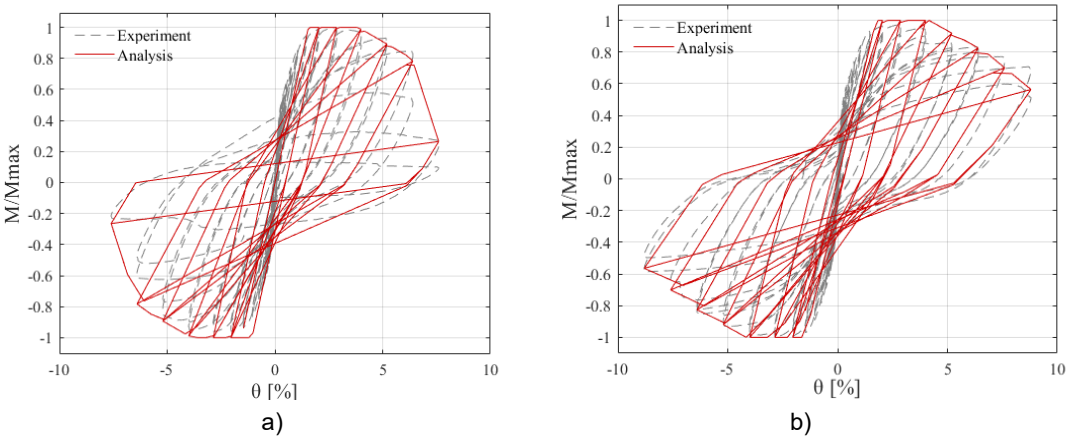

Figure 12. Results of numerical analysis for columns a) SUB/90 and b) STD/135

5 Conclusions

Different procedures for estimating the NC rotation included in Eurocode 8 (current versions of Eurocode 8/3 [25], Eurocode 8/2 [26], and the draft of the new version of Eurocode 8/1 [27]) were compared and evaluated by cyclic experiments of well- and poorly-confined RC columns with rectangular cross-sections.

Some procedures predicted the response of substandard columns well but were less effective for standard columns, while others had the opposite results. The only effective procedure in both cases was the empirical procedure included in Eurocode 8/3.

The NC rotation estimated according to the Eurocode 8/3 empirical procedure was used as a basis to define several trilinear and quadrilinear moment–rotation backbone models. These were verified against the experiments, and the most suitable model was identified.

The models proposed in the literature for columns with a certain level of confinement may not be generally suitable. The generality of a model can be improved by increasing the number of branches in the post-capping part of the backbone. The best match for both types of columns was obtained using the quadrilinear backbone model defined by: (i) the Haselton capping rotation [10], (ii) the Eurocode 8/3 NC rotation, and (iii) the TC rotation proposed by Anžlin for quadrilinear backbones [23].

This quadrilinear backbone model is proposed for simulating the seismic response of reinforced concrete elements with predominantly flexural behaviour. The results suggest that the model can be applied generally regardless of the seismic design level of the structure, which is a useful feature when analysing a portfolio of structures constructed in different periods. Moreover, the proposed model simulates the seismic response at various intensity levels up to the point of TC, making it suitable for studies to estimate the risk of casualties.

However, only a limited number of columns were considered in this study. Extension of the presented study is needed, and it is planned to be performed soon. Moreover, further research is needed to evaluate the impact of the modelling uncertainty associated with the simulation of the post-capping response on the risk of casualties, as this would help to better understand the significance of appropriate modelling of the post-capping region.

Acknowledgements

The research presented in this paper is based on work sponsored by the Slovenian Research Agency, which is gratefully acknowledged. The authors would also like to thank Andrej Anžlin from the Slovenian National Building and Civil Engineering Institute for his help.

References

[1] Takeda T, Sozen M. A, Nielsen N. N. Reinforced concrete response to simulated earthquakes. Journal of Structural Division 96, 1970, 12: 2557–2573, https://doi.org/10.1061/JSDEAG.0002765.

[2] Allahabadi R, Powell G. H. DRAIN-2DX: user guide. Berkeley, the United States: Earthquake Engineering Research Center, University of California, 1988.

[3] Kunnath S. K, Reinhorn A. M, Park Y. J. Analytical modeling of inelastic seismic response of R/C structures. Journal of Structural Engineering116, 1990, 4: 996-1017, https://doi.org/10.1061/(ASCE)0733-9445(1990)116:4(996).

[4] Dymiotis C, Kappos A. J, Chryssanthopoulos M. K. Seismic reliability of RC frames with uncertain drift and member capacity. Journal of Structural Engineering 125, 1999, 9: 1038-1047, https://doi.org/10.1061/(ASCE)0733-9445(1999)125:9(1038).

[5] Pincheira J, Dotiwala F. S, D'Souza J. T. Seismic analysis of older reinforced concrete columns. Earthquake Spectra15, 1999, 2: 245-272, https://doi.org/10.1193/1.1586040.

[6] Blasone V, Basaglia A, De Risi R, De Luca F, &Spacone E. A simplified model for seismic safety assessment of reinforced concrete buildings: framework and application to a 3-storey plan-irregular moment resisting frame. Engineering Structures, 250, 2022, 113348,https://doi.org/10.1016/j.engstruct.2021.113348

[7] D'Angela D, Magliulo G, Celano F, & Cosenza E. Characterization of local and global capacity criteria for collapse assessment of code-conforming RC buildings. Bulletin of Earthquake Engineering 19, 2021, 9: 3701-3743, https://doi.org/10.1007/s10518-021-01115-y

[8] Bayari M A, Shabakhty N, & Abadi E I Z. Analyzing uncertainties involved in estimating collapse risk with and without considering uncertainty probability distribution parameters. Earthquake engineering and engineering vibration, 2022, 1-16. https://doi.org/10.1007/s11803-021-2068-x

[9] Panagiotakos T. B, Fardis M. N. Deformations of reinforced concrete members at yielding and ultimate. Structural Journal, 98, 2001, 2: 135-148. https://doi.org/10.14359/10181.

[10] Haselton C. B. Assessing Seismic collapse safety of modern reinforced concrete modern frame buildings. PhD Thesis. Stanford, CA, USA: Stanford University, 2006.

[11] Singhal A, Kiremidjian A. S. Method for probabilistic evaluation of seismic structural damage. Journal of structural Engineering122, 1996, 12: 1459-1467, https://doi.org/10.1061/(ASCE)0733-9445(1996)122:12(1459).

[12] Melani A, Khare R. K, Dhakal R. P, Mander J. B. Seismic risk assessment of low rise RC frame structure. Structures 5, 2016, 13-22, https://doi.org/10.1016/j.istruc.2015.07.003.

[13] Babič A, Dolšek M. Seismic fragility functions of industrial precast building classes. Engineering structures118, 2016, 357-370, https://doi.org/10.1016/j.engstruct.2016.03.069.

[14] Suselo A. A. Simulated Behavior of Rectangular Reinforced Concrete Columns under Seismic Loading. Doctoral dissertation, The University of Texas at San Antonio, 2021.

[15] Eldawie A. Collapse Modeling of Reinforced Concrete Frames Under Seismic Loading. Doctoral dissertation, Ohio State University, 2020.

[16] ASCE/SEI. Seismic rehabilitation of existing buildings (ASCE/SEI 41-17). Reston, VA, 2017, 623pp

[17] Fischinger M, Kramar M, Isaković T. Cyclic response of slender RC columns typical of precast industrial buildings. Bulletin of earthquake engineering6, 2008, 3: 519-534, https://doi.org/10.1007/s10518-008-9064-7.
[18] Jalayer F, Ebrahimian H. Seismic risk assessment considering cumulative damage due to aftershocks. Earthquake Engineering & Structural Dynamics46, 2017, 3: 369-389, https://doi.org/10.1002/eqe.2792.
[19] Dolšek M, Fajfar P. Mathematical modelling of an infilled RC frame structure based on the results of pseudo-dynamic tests. Earthquake engineering & structural dynamics31, 2002, 6: 1215-1230, https://doi.org/10.1002/eqe.154.
[20] Ibarra L. F, Medina R. A, Krawinkler H. Hysteretic models that incorporate strength and stiffness deterioration. Earthquake Engineering & Structural Dynamics 34, 2005, 12:1489–1511, https://doi.org/10.1002/eqe.495.
[21] Verderame G. M, Polese M, Mariniello C, Manfredi G. A simulated design procedure for the assessment of seismic capacity of existing reinforced concrete buildings. Advances in Engineering Software41, 2010, 2: 323-335, https://doi.org/10.1016/j.advengsoft.2009.06.011.
[22] Kreslin M, Fajfar P. Seismic evaluation of existing complex RC building. Bulletin of Earthquake Engineering 8, 2010, 2: 363–385, https://doi.org/10.1007/s10518-009-9155-0.
[23] Anžlin A. Influence of buckling of longitudinal reinforcement in columns on seismic response of existing reinforced concrete bridges. PhD Thesis. Ljubljana, Slovenia: University of Ljubljana, 2017.
[24] Di Domenico M, Ricci P, Verderame GM. Empirical calibration of hysteretic parameters for modeling the seismic response of reinforced concrete columns with plain bars. Eng Struct, 2021, 237:112120, https://doi.org/10.1016/j.engstruct.2021.112120
[25] CEN. Eurocode 8: Design of structures for earthquake resistance – Part 3: Assessment and retrofit of buildings. ComitéeEuropéeen de Normalisation (EN 1998-3:2005). Brussels, Belgium, 2005.
[26] CEN. Eurocode 8: Design of structures for earthquake resistance – Part 2: Bridges. ComitéeEuropéeen de Normalisation (EN 1998-2:2005). Brussels, Belgium, 2005.
[27] CEN. Eurocode 8: Design of structures for earthquake resistance – Part 1-1: General rules and seismic actions. Working draft by project team SC8 2021-02-17, CEN TC 250 work programme. ComitéEuropéen de Normalisation (prEN 1998-1:2020). Brussels, Belgium, 2020.
[28] CEN. Eurocode 2: Design of concrete structures – Part 1-1: General rules and rules for buildings. ComitéeEuropéeen de Normalisation (EN 1991-1:2005). Brussels, Belgium, 2005.
[29] McKenna F, Fenves G. L, Scott M. H. Open system for earthquake engineering simulation. University of California, Berkeley, 2000. http://opensees.berkeley.edu.
[30] Žižmond J, Podgorelec D, Dolšek M. Relationship between the collapse risk and the reinforced concrete frame structure. In Second European conference on earthquake engineering and seismology. Istanbul, Turkey, 2014.
[31] Dolšek M. Development of computing environment for the seismic performance assessment of reinforced concrete frames by using simplified nonlinear models. Bulletin of Earthquake Engineering 8, 2010, 6: 1309–1329, https://doi.org/10.1007/s10518-010-9184-8.
[32] Zevnik J. Potresna ranljivost armiranobetonskih viaduktov s škatčastimistebri. PhD Thesis. Ljubljana, Slovenia: University of Ljubljana, 2007.